Journal of Solid State Chemistry **153,** 386–390 (2000)
doi:10.1006/jssc.2000.8787, available online at http://www.idealibrary.com on IDEAL®

Reaction Mechanism of Metal Silicide Mg_2Si for Li Insertion

Toshihiro Moriga,[1] Kozo Watanabe, Daisuke Tsuji, Shinichi Massaki, and Ichiro Nakabayashi

Department of Chemical Science and Technology, Faculty of Engineering, The University of Tokushima, 2-1 Minami-Josanjima, Tokushima 770-8506, Japan

Received February 1, 2000; in revised form May 19, 2000; accepted May 26, 2000; published online July 7, 2000

Electrochemical Li insertion into the anti-fluorite-type Mg_2Si was performed and the structural variation during the insertion was examined. It was found that lithium insertion into Mg_2Si proceeds stepwise according to the following reactions: $Mg_2Si+2Li^++2e^- \rightarrow Li_2MgSi+Mg$, and $Mg+yLi^++ye^- \rightarrow Li_yMg$. Li_2MgSi has the $2a_F\times2a_F\times2a_F$ structure with space group *Fm*-3*m*, where a_F represents a lattice length of the fundamental fluorite unit cell. DV-*X*α calculation showed that charge compensation in Mg_2Si accompanied by the Li insertion into the vacant octahedral site occurs by indroduction of electrons into Mg3*s* orbitals, resulting in a reduction of Mg^{2+} ions. Thus, one-half of the Mg^{2+} ions discharge from Mg_2Si and the Li^+ ion is incorporated into the missing site to form Li_2MgSi. © 2000 Academic Press

Key Words: **fluorite-type structure; Li insertion; X-ray diffractometry; DV-*X*α calculation.**

1. INTRODUCTION

Secondary lithium cells have been of great interest among battery researchers and electrochemists. Great efforts have been made toward finding novel candidate electrode materials for the lithium cells. A material with the fluorite-type structure is one promising electrode material since it has the flexibility to be nonstoichiometric to some extent and/or has a capacity to store guest ions such as Li^+ at the vacant 4(*b*) octahedral site. Nonoxides with the fluorite-type structure, such as Li_3FeN_2 and Li_7MnN_4 which have the anti-fluorite-type superstructure, have been reported as new electrode materials for lithium secondary batteries (1,2).

Metal silicide alloys are thought to be suitable for lithium batteries because Si has a good affinity to Li and they would easily incorporate Li into their structure. Mg_2Si is reported to be a semiconductor (3) and takes the cubic anti-fluorite-type structure where Si occupies the octahedral site to form the fcc arrangement and Mg occupies the tetrahedral site. Its related compound $Li_{2-2x}Mg_{1+x}Si$ has been reported as a superionic conductor (4,5). When Li can be intercalated into the 4(*b*) octahedral site in Mg_2Si to form $LiMg_2Si$, its specific capacity can be calculated to be as high as 350 mA h/g. As Mg_2Si has cell dimensions of $a = 6.351$ Å (6), the void at the 4(*a*) site would be large enough to store guest Li^+ ions. Anani and Huggins (7,8) have reported electrochemical coulometric titration for the ternary Li–Si–Mg alloy at current densities of 5–20 mA/cm^2. However, they showed that the three-phase equilibrium can be represented by the reaction, $4Mg_2Si + 13Li \Leftrightarrow 8Mg + Li_{13}Si_4$, which means in no phase can such as $LiMg_2Si$ can be obtained. This fact is in conflict with the existence of $Li_{2-2x}Mg_{1+x}Si$ (4,5).

In this paper, electrochemical Li insertion into Mg_2Si was conducted under milder conditions with a current density as low as 0.5 mA/cm^2 and the structural variation during the insertion was examined by X-ray diffractometry, X-ray photoelectron spectroscopy, and DX-*X*α calculation.

2. EXPERIMENTAL

The starting material was granular Mg_2Si (High Purity Chemicals, Japan). The Mg_2Si was ground in an Ar atmosphere by a p-7 planetary ball mill (Fritsch, Idar-Oberstein, Germany) at 3400 rpm for 25 seconds. A 25 ml stainless jar and seven balls 12 mm in diameter of tungsten carbide were used for grinding. The amount of powder loaded was 3 g. The grain size of Mg_2Si after griding was less than 30 μm.

The ground Mg_2Si was mixed with acetylene black (AB) as an electron conductor and 12 wt% poly(vinylidene fluoride) (PVDF) solution dissolved in *N*-methyl-2-pyrrolidone (NMP) as a binder (Mg_2Si : AB : PVDF solution = 100 : 4 : 40). The mixture was pasted on Cu foil, dried at 100°C overnight to remove the NMP, and then pressed into a sheet. Using this sheet as a cathode, an Li sheet as an anode, and 1 M $LiPF_6$/dimethyl carbonate (DMC) + diethyl carbonate (DEC) (DMC : DEC = 1 : 1) as the electrolyte, the cell was assembled. Electrochemical lithium insertion was performed by the three-electrode method at a constant current density of 0.5 mA/cm^2 at room temperature. The amount of Li inserted was coulometrically

[1] To whom correspondence should be addressed. Fax: 81-88-655-7025. E-mail: moriga@chem.tokushima-u.ac.jp.

0022-4596/00 $35.00

calculated. All the electrochemical treatments of the samples were carried out in an Ar-filled drybox. P_2O_5 was used as desiccant. The samples were washed with DEC several times prior to the measurements described below.

XRD measurements were performed on a Rigaku RINT2500VHF + diffractometer using monochromatized Cu$K\alpha$ radiation (50 kV, 100 mA). As the products were sensitive to air, they were protected against exposure to air by using a hand-made holder filled with Ar gas. The window of the holder was covered with a commercial cellophane tape. Simulations of X-ray diffraction pattern of the products were conducted with use of the software RIETAN94 (9).

X-ray photoelectron spectroscopy (XPS) measurements were conducted on a Shimadzu ESCA-1000 device using Mg$K\alpha$ radiation (10 kV, 30 mA). The specimens were mounted in the form of a 3 mm diameter pellet. The resolution of the concentric hemispherical analysis was higher than 0.1 eV. Neither smoothing nor calibration of binding energy was done. Prior to the measurements, Ar-etching of the sample was carried out at a source power of 2 kV, 20 mA for 6 seconds.

The DV-$X\alpha$ method was employed for the calculation of density of states (DOS) in the vicinity of the Fermi level in Mg_2Si. The calculations were carried out with the software SCAT (10,11). The cluster model of Mg_2Si was designed with $[Mg_{32}^{2+}Si_{14}^{4-}]^{8+}$ having $m3m$ symmetry on the basis of the structure of Mg_2Si ($a = 6.351$ Å) so that the cluster is spherical and the 4(b) site is at the center of the cluster. Numerical atomic orbitals of 1s to 3p for Mg and Si were used as a basis set for the calculations. The radius and depth of the well potential used were 2.5 a.u. (atomic units, 1 a.u. = 0.529 Å) and -1.5 eV, respectively. The sample points used in the numerical integration were taken up to 10,000 for each calculation. Self-consistency within 0.001 electrons was obtained for the final populations. Simulation of the XPS spectrum was done by multiplying the orbital population obtained from the DOS calculation by the photoelectron emission coefficient of the given atoms (12).

3. RESULTS AND DISCUSSIONS

Figure 1 shows the initial discharge curve for the Li/Li_xMg_2Si cell. The electrochemical insertion was performed until $x = 3.82$ in Li_xMg_2Si. At the time when the circuit was completed, the voltage dropped rapidly, then increased gradually up to 0.11 V, and remained constant until $x \simeq 2.0$. One possibile cause of the initial voltage drop, the so-called IR drop, is low activity of the Mg_2Si ($x = 0$) electrode. The initial electrochemical insertion would proceed very slowly. Anani and Huggins (8) have pointed out that such drops are associated with nucleation of new phases as the addition or removal of the electroactive species moves the equilibrium. When the electrode reactions attained equilibrium, the voltage recovered up to 0.11 V. Afterward, the voltage decreased asymptotically to 0 V.

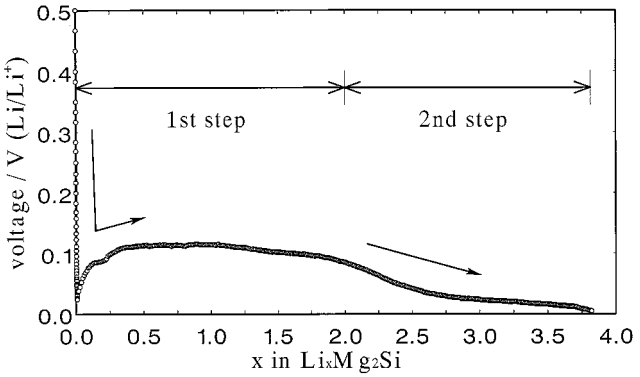

FIG. 1. Initial discharge curve for Li/Li_xMg_2Si cell.

These appeared to be two steps in the curve. The first step lay in the range of $0 < x \leq 2.0$, and the second one lay in the range of $x > 2.0$.

In the range of $x = 0.50$ to 1.50, diffraction peaks assigned to hexagonal Mg metal were observed in addition to those assigned to Mg_2Si, as shown in Fig. 2. The diffraction patterns in the 2θ range from 38° to 42° after magnification are shown on the right side of Fig. 2. Upon increasing the

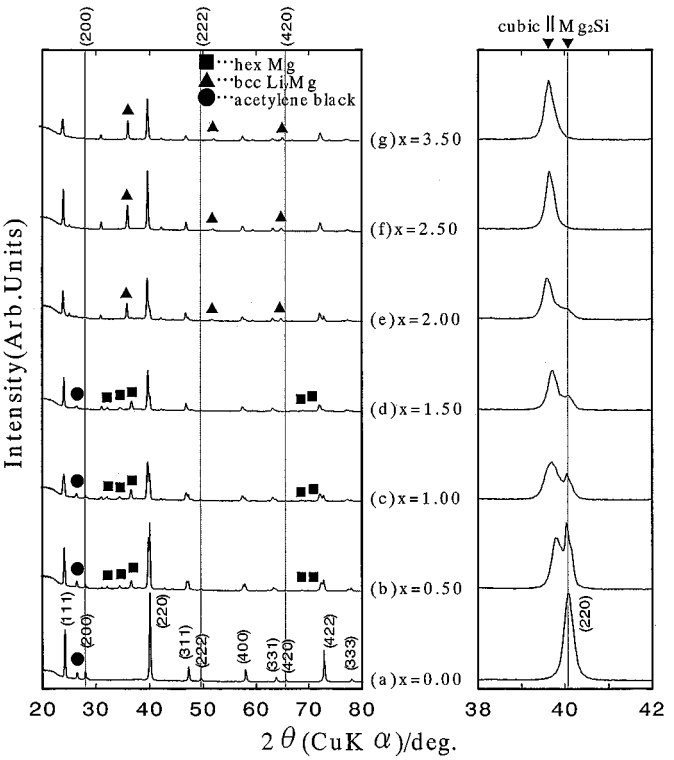

FIG. 2. Variation of X-ray diffraction patterns for Li-inserted Mg_2Si. "x" shows the amount of inserted Li in Li_xMg_2Si. A magnified X-ray diffraction pattern in the 2θ range from 38° to 42° for each specimen is also shown on the right side.

amount of Li insertion, the intensity of the peaks assigned to the Mg_2Si phase gradually decreased, and a new phase having slightly larger cell dimensions than the Mg_2Si phase (abbreviated as cubic II phase hereafter) appeared and its peaks increased in intensity. The *a*-lengths of both the Mg_2Si and the cubic II phases did not change during the Li insertion (e.g., $a = 6.346(3)$ Å at $x = 0$, $a = 6.35(1)$ Å at $x = 0.5$, and $a = 6.35(2)$ Å at $x = 2.0$ for Mg_2Si, and $a = 6.39(1)$ Å at $x = 0.5$, $a = 6.40(2)$ Å at $x = 2.0$, and $a = 6.40(1)$ Å at $x = 3.5$ for cubic II, respectively). Interestingly, the (200), (222), and (420) peaks of Mg_2Si diminished with increasing *x*. According to the simulations of X-ray diffraction patterns of $Mg_{2-\delta}Si$ with the imaginary anti-fluorite-type structure, the half-occupation probability of Mg at the 8(*c*) site (i.e., $\delta = 0.5$) leads these peaks to vanish. These results imply that the Mg_2Si phase discharges half of the Mg metal to form the cubic II phase. The metal ratio of Mg : Si in the cubic II phase should be 1 : 1.

At $x = 2.00$, the hexagonal Mg phase disappeared and a body-centered cubic Li phase suddenly appeared. The lattice constant of the bcc phase seemed to converge to $a = 3.509$ Å, which is the *a*-length of Li metal, with an increase of *x* (e.g., $a = 3.55(2)$ Å at $x = 2.00$, $a = 3.53(1)$ Å at $x = 2.5$, and $a = 3.51(1)$ Å at $x = 3.5$). The diffraction peaks assigned to the Mg_2Si phase could be seen at $x = 2.00$, but disappeared at $x = 2.50$. The amounts of both the cubic II and the bcc phases were unchanged from $x = 2.5$ up to $x = 3.88$. Two equivalents of lithium would react with one equivalent of Mg_2Si to form the cubic II phase. Considering the electrochemical measurements (Fig. 1) and XRD ones (Fig. 2), the lithium insertion into Mg_2Si would proceed stepwise as follows:

$$Mg_2Si + 2Li^+ + 2e^- \rightarrow Li_2MgSi \text{ (cubic II)} + Mg \quad [1]$$

$$Mg + yLi^+ + ye^- + Li_yMg. \quad [2]$$

In the range of $0 < x < 2.0$ (first step in Fig. 1), the Li insertion into Mg_2Si and the Mg extraction from Mg_2Si take place simultaneously to form Li_2MgSi, denoted as Eq. [1]. Li_2MgSi is the end-member of $Li_{2-2x}Mg_{1+x}Si$ solid solutions, reported by Wengert *et al.* (4). No $Li_{13}Si_4$ phase, which Anani and Huggins (8) have reported as one of the products of Li insertion into Mg_2Si, was observed. It would result from the lower applied current density in this work, so that a complete extraction of magnesium from Mg_2Si and a reaction between the resultant silicon and lithium would be avoidable. At the second step in Fig. 2, the extracted Mg reacts with lithium to form Li_yMg alloy, denoted as Eq. [2]. The reason the Mg_2Si did not entirely disappear at $x = 2.0$ is that reaction [2] would begin before reaction [1] was completed.

Wengert *et al.* (4) also have proposed two possible structural models for Li_2MgSi (cubic II) as tabulated in Table 1. One (model 1) has the $a_F \times a_F \times a_F$ structure with space group *P*-43*m* and the other (model 2) has the $2a_F \times 2a_F \times 2a_F$ structure with space group *Fm*-3*m*, where a_F represents a lattice length of the fundamental fluorite unit cell. As for the results of Rietveld simulation, several weak peaks could not be indexed when model 1 was used. Model 2 could explain the experimental pattern successfully. Experimental and simulated X-ray diffraction patterns for Li_2MgSi obtained by using model 2, together with those for LiMg (by-product), are shown in Fig. 3. The schematic representation of the structure for Li_2MgSi (model 2) is shown in Fig. 4. Li_2MgSi comprizes the face-centered cubic arrangement of silicons. The inserted lithiums occupy half of the 8(*c*) site by substituting Mg in addition to the 4(*a*) site on the basis of the fluorite-type structure. The structure of Li_2MgSi is made up of the combination of two types of Li_2MgSi units. Rotating one Li_2MgSi unit for 90° clockwise about the *a*-axis can make the other Li_2MgSi unit. The two units are alternatively arranged. The edge-shared tetrahedrons

TABLE 1
Two Possible Structural Models for Li_2MgSi Proposed by Wengert *et al.* (4)

Model 1					Model 2				
Space group lattice parameter		*P*-43*m* (No. 215) $a = 6.415$ Å			Space group Lattice parameter		*Fm*-3*m* (No. 225) $a = 12.830$ Å		
Atom	Site	Position			Atom	Site	Position		
		x	*y*	*z*			*x*	*y*	*z*
Si(1)	1(*a*)	0	0	0	Si(1)	4(*a*)	0	0	0
Si(2)	3(*c*)	1/2	1/2	0	Si(2)	4(*b*)	1/2	1/2	1/2
					Si(3)	24(*d*)	0	1/4	1/4
Li(1)	1(*b*)	1/2	1/2	1/2	Li(1)	8(*c*)	1/4	1/4	1/4
Li(2)	3(*d*)	1/2	0	0	Li(2)	24(*e*)	0.25	0	0
Li(3)	4(*e*)	0.25	0.25	0.25	Li(3)	32(*f*)	0.125	0.125	0.125
Mg	4(*e*)	0.75	0.75	0.75	Mg	32(*f*)	0.375	0.375	0.375

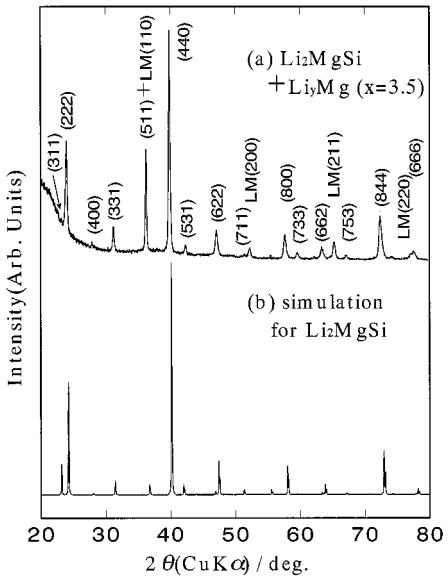

FIG. 3. (a) Experimental and (b) simulated X-ray diffraction patterns for Li_2MgSi (the amount of inserted Li $x = 3.5$) obtained by using model 2. L*M* represents Li_yMg (by-product).

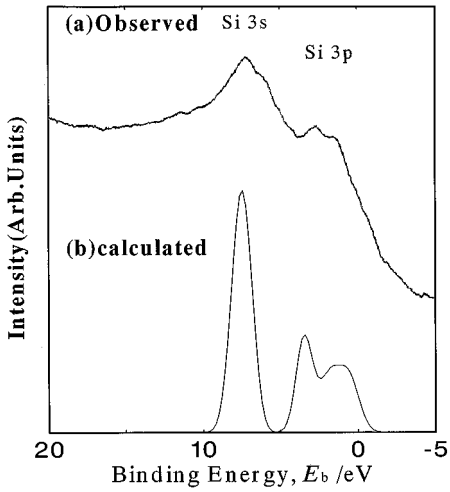

FIG. 5. Calculated XPS spectrum for Mg_2Si near the valence region obtained by using the DV-$X\alpha$ method in comparison with the experimental spectrum.

occupied by Li are arranged so that they are adjacent to those occupied by Mg in the respective unit.

Figure 5 shows the calculated XPS spectrum for the Mg_2Si near valence region obtained by using the DV-$X\alpha$ method in comparison with the experimental spectrum. The experimental spectrum had two peaks in this region. The peak with the lower binding energy was attributed to Si3*p* and Mg3*s* and that with the higher binding energy was attributed to Si3*s*. The theoretical spectrum obtained from the calculation is in good agreement with the experimental one. Figure 6 shows the calculated DOS for Mg_2Si. The HOMO (highest occupied molecular orbital) is mainly composed of Si3*p*, and Mg3*s* is the main component of the LUMO (lowest unoccupied molecular orbital). The latter fact indicates that charge compensation in Mg_2Si accompanied by Li insertion would be performed by indroduction of electrons into Mg3*s* orbitals forming the LUMO. This kind of concept has been proposed by Okamura (13). The introduction of electrons into Mg3*s* orbitals results in a reduction of Mg^{2+} ions. Insertion of one Li^+ ion should induce the reduction of one Mg^{2+} ion to Mg^+. The Mg^+ is,

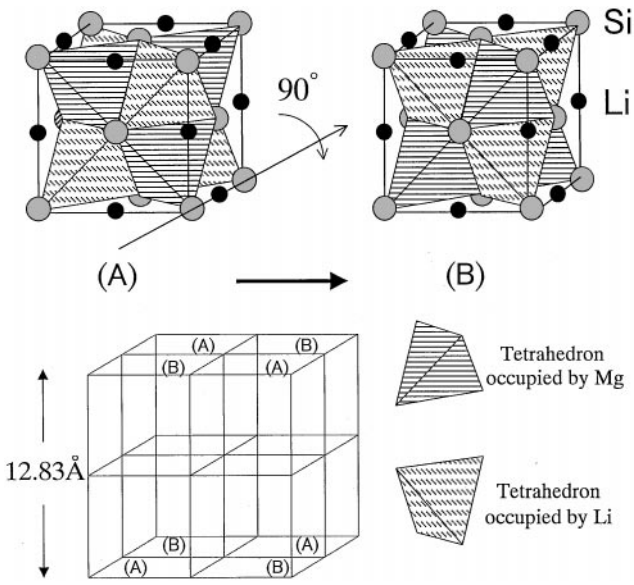

FIG. 4. Schematic representation of the structure for Li_2MgSi (model 2).

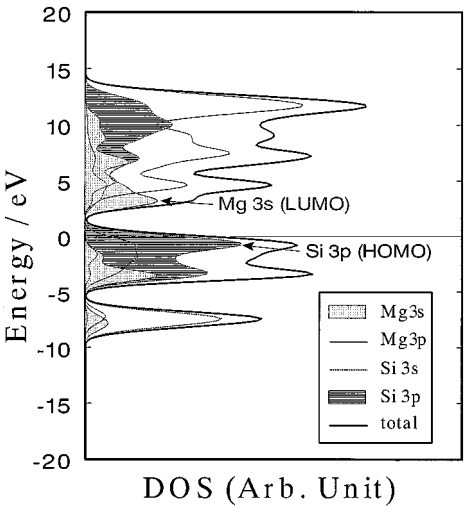

FIG. 6. Calculated density of state (DOS) for Mg_2Si obtained by using the DV-$X\alpha$ method.

however, so unstable that one Mg^{2+} ion discharges from Mg_2Si and the additional Li^+ ion is incorporated into the missing site. Thus, the above-mentioned reaction ($Mg_2Si + 2Li^+ + 2e^- + Li_2MgSi + Mg$) proceeds at an early step of the Li insertion.

It is convenient that the Mg site in the anti-fluorite-type structure is the first neighbor of the 4(*b*) site the inserted Li^+ ions occupy. Electrons introduced into the Mg3*s* orbital can directly perform charge compensation accompanied by Li insertion. We have clarified that Li insertion into $NiSi_2$ cannot be done (14). In $NiSi_2$, the Si site is the first neighbor of the 4(*b*) site whereas the LUMO is mainly composed of Ni3*d* orbitals. For Li insertion into metal silicides to occur, it would be necessary that the species contibuting the LUMO are identical to the species adjacent to the Li-introduced sites.

ACKNOWLEDGMENTS

The authors thank Mr. K. Okamura of Matsushita Battery Industry Co. Ltd. for technical assistance and useful suggestions in DV-$X\alpha$ calculations. This work was partly supported by a research grant from Matsushita Battery Industry Co. Ltd., and by a Grant-in-Aid for Scientific Research from the Ministry of Education, Science, and Culture.

REFERENCES

1. M. Nishijima, Y. Takeda, N. Imanishi, and O. Yamamoto, *J. Solid State Chem.* **113,** 205 (1994).
2. M. Nishijima, N. Tadokoro, Y. Takeda, N. Imanishi, and O. Yamamoto, *J. Electrochem. Soc.* **141,** 2966 (1994).
3. R. J. LaBotz, D. R. Mason, and D. F. O'Kane, *J. Electrochem. Soc.* **110,** 127 (1967).
4. S. Wengert, R. Nesper, W. Andreoni, and M. Parrinello, *Phys. Rev. Lett.* **77,** 5083 (1996).
5. R. Nesper and J. Curda, *Z. Kristallogr.* **182,** 196 (1988).
6. "Constitution of Binary Alloys, 2nd Edition" (M. Hansen and K. Anderko, Eds.), pp. 916–918. Genium Publishing, New York, 1985.
7. A. Anani and R. A. Huggins, *J. Power Sources* **38,** 351 (1992).
8. A. Anani and R. A. Huggins, *J. Power Sources* **38,** 363 (1992).
9. F. Izumi, *in* "The Rietveld Method" (R. A. Young, Ed.), pp. 236–253. Oxford Univ. Press, Oxford, 1995.
10. H. Adachi, M. Tsukada, and C. Satoko, *J. Phys. Soc. Jpn.* **45,** 875 (1978).
11. "Hajimete-no-Denshi-Jotai-Keisan (Introduction to Electronic State Calculations)" (H. Adachi, Ed.). Sankyo-Shuppan, Tokyo, 1998 (in Japanese).
12. J. J. Yeh and I. Lindau, *At. Data Nucl. Data Tables* **32,** 1 (1985).
13. K. Okamura, *Bull. Soc. Discrete Variational* $X\alpha$ **10,** 116 (1997) (in Japanese).
14. K. Watanabe, Master Thesis, Dept. of Chem. Sci. & Tech., The University of Tokushima, 1999.